Journal of Materials Research and Technology 40 (2026) 188–193

Contents lists available at ScienceDirect

Journal of Materials Research and Technology

journal homepage: www.elsevier.com/locate/jmrt

Identification of lattice defects in laser powder bed fusion-fabricated 316L stainless steel by positron annihilation spectroscopy

Masataka Mizuno [a,*], Masaki Otsuka [a], Kazuhisa Sato [b], Takuya Ishimoto [a,c,d], Takayoshi Nakano [a,c], Hideki Araki [a]

[a] Division of Materials and Manufacturing Science, Graduate School of Engineering, The University of Osaka, 2-1 Yamadaoka, Suita, Osaka, 565-0871, Japan
[b] Research Center for Ultra-High Voltage Electron Microscopy, The University of Osaka, 7-1 Mihogaoka, Ibaraki, 567-0047, Japan
[c] Anisotropic Design and Additive Manufacturing Research Center, The University of Osaka, 2-1, Yamadaoka, Suita, Osaka, 565-0871, Japan
[d] Aluminium Research Center, University of Toyama, 3190, Gofuku, Toyama, 930-8555, Japan

ARTICLE INFO

Keywords:
Laser powder bed fusion
316L stainless steel
Positron annihilation
Vacancies
Dislocations

ABSTRACT

The laser powder bed fusion (LPBF) process often introduces lattice defects, such as vacancies and dislocations, within the fabricated materials because of large thermal gradients and rapid cooling rates. In this study, lattice defects in LPBF-fabricated 316L stainless steel (SS) were quantitatively evaluated using positron annihilation spectroscopy, a sensitive technique for detecting and characterizing vacancies and dislocations. The number of lattice defects increased with the LPBF scan speed. Vacancy concentrations and dislocation densities were determined using component analysis of the positron lifetime spectra. The measured vacancy concentration was comparable to the thermal equilibrium concentration of vacancies at the melting point. Additionally, both vacancy concentration and dislocation density increased with scan speed. The increase in dislocation density in the fabricated 316L SS with increasing scan speed of the LPBF process was confirmed using transmission electron microscopy. This study enables the detection and identification of defects in 316L SS under various temperature conditions, offering insights into the performance of 316L SS across a wider range of operating temperatures.

1. Introduction

Laser powder bed fusion (LPBF) is widely considered a promising additive manufacturing technique. It is characterized by the melting of powder layers, followed by rapid solidification at high cooling rates of 10^5–10^7 K/s. Therefore, quenched-in vacancies are expected to be introduced during the process owing to these high cooling rates [1,2]. Positron lifetime spectroscopy is an effective technique for the quantitative evaluation of vacancy-type defects. In a perfect crystal, the positron wave function is delocalized in the interstitial regions due to repulsion from the ion cores. When vacancy-type defects, such as monovacancies, vacancy clusters or dislocations, are present, the positron wave function becomes localized at these sites where the local electron density is lower than in the interstitial regions. This localization leads to an increase in positron lifetime relative to the bulk value, as the positron lifetime is inversely proportional to the electron density at the annihilation site [3]. Furthermore, because different vacancy-type defects exhibit characteristic positron lifetimes, quantitative defect analysis can be achieved through component analysis of the measured lifetime spectra [4,5]. In our previous study, positron lifetime measurement was performed to identify the lattice defects in an LPBF-fabricated β-type Ti–15Mo–5Zr–3Al [6]; however, vacancy-type defects were not observed in the as-fabricated samples. Furthermore, the results of first-principles calculations performed on Ti–Mo binary alloys suggested that stabilization of the body-centered structure by Mo atoms is not sufficient to introduce quenched-in vacancies during the LPBF process [6]. In contrast, Xunxiang et al. [7] reported on the presence of dislocations and monovacancies, detected using positron lifetime measurements, in an LPBF-fabricated 316L stainless steel (SS). However, the number of detected lattice defects was not quantified because the lifetime components of the lattice defects were not decomposed into dislocations and monovacancies.

316L SS is a widely used structural material, and the lattice defects introduced in LPBF-fabricated 316L SS during LPBF processing have been extensively studied [8–19]. Dislocations introduced in LPBF-fabricated 316L SS are considered a major contributor to its superior tensile properties compared with conventionally manufactured counterparts [8–13,19]. Kernel average misorientation analyses have

* Corresponding author.
E-mail address: mizuno@mat.eng.osaka-u.ac.jp (M. Mizuno).

https://doi.org/10.1016/j.jmrt.2025.12.147
Received 14 May 2025; Received in revised form 8 December 2025; Accepted 14 December 2025
Available online 15 December 2025

shown that dislocation strengthening accounts for the largest proportion of the yield-strength enhancement in LPBF-produced alloys [19]. The thermal stability of the dislocation cell structures has been examined through heat treatments of as-fabricated samples [11–13,17]. A reduction in tensile yield stress has been reported when annealing above 973 K, primarily due to the corresponding decrease in dislocation density [11]. Experimental investigations of dislocation evolution and its influence on hardness during annealing indicate that the hardness of LPBF-fabricated 316L SS is governed predominantly by geometrically necessary dislocations [12]. Compared with conventionally deformed 316L samples, LPBF-fabricated 316L SS exhibits a lower recovery rate during annealing and requires a higher apparent activation energy for recovery, attributed to the pinning effect associated with solute-segregation networks [17]. Transmission electron microscopy (TEM) studies have revealed dislocation cell structures enriched with segregated Cr and Mo in LPBF-fabricated 316L SS [8,9], with quantitative analyses indicating segregation levels of approximately 1–2 wt% [14]. Thermal stress analyses have further suggested that the formation of dislocation structures originates from the thermal distortions imposed during LPBF processing [10]. Additionally, nanoscale modulated structures arising from elastic strain within dislocation cells have been documented [15]. In contrast to the extensive research on dislocation formation and evolution, the introduction of vacancies in LPBF-manufactured 316L SS has remained comparatively understudied, despite their significant implications for solute diffusion, precipitation kinetics, and creep deformation.

In this study, to quantitatively evaluate the quenched-in vacancies and dislocations in LPBF-fabricated 316L SS, positron lifetime measurements were performed on as-fabricated and isochronally annealed samples. Additionally, the effect of scan speed on the vacancy concentration and dislocation density in 316L SS was examined.

2. Experimental method

Rectangular samples with bottom dimensions of 10 mm × 10 mm were fabricated using an LPBF apparatus (EOS M290, EOS, Germany) with a bidirectional Yb fiber laser scan along the x-axis. The nominal composition of the 316L SS powder was 18Cr–14Ni-2.5Mo-0.03C (wt. %).

To evaluate the influence of fabrication parameters on the positron lifetime, the scan speed of the LPBF process was varied in the range 400–1400 mm/s, while the laser power was kept constant at 250 W. Details of the LPBF process are described in an earlier study [20]. The recovery of lattice defects was observed by isochronally annealing the as-fabricated samples for 1 h at temperatures in the range 373–873 K, with the temperature increased in steps of 25 K. The bulk positron lifetime of the fabricated 316L SS was determined using solution-treated samples prepared by air cooling after holding the as-fabricated samples at 1423 K for 3 h.

Positron lifetime measurements were performed using a digital oscilloscope (Lecroy WaveRunner 62-Xi), with a time resolution of 187.8 ps and photomultiplier tubes equipped with BaF_2 scintillators. The positron lifetime spectra were obtained at a coincidence count rate of 45 counts per second and a total coincidence count of 3×10^6. The resulting positron lifetime spectra were analyzed using the Resolution [21] and Positronfit Extended [22] programs. The positron annihilation lifetime spectrum of each sample was decomposed into one to three components, as necessary. The mean positron annihilation lifetime was calculated using a two-state trapping model [23], using a defect-free defect component. Plan-view TEM specimens were fabricated by lapping and polishing the samples along the YZ-plane (the build direction was defined as the Z-axis) using a focused ion beam (FIB) instrument (ThermoFischer Scientific Scios2 DualBeam) equipped with Ga ions. Microstructures of the fabricated TEM specimens were characterized using scanning transmission electron microscopy (STEM) on a JEOL JEM-ARM200F TEM operated at 200 kV. The thicknesses of the TEM specimens required for dislocation density evaluation were measured by electron energy-loss spectroscopy (EELS) with a Gatan ContiniumK3 post-column energy filter.

3. Results and discussion

The positron lifetimes of the as-fabricated samples increase with scan speed and are more than 50 ps longer than that of the bulk positron lifetime (104 ps) (Fig. 1). The lifetimes of the positrons trapped at lattice defects, such as vacancies and dislocations, are longer than those of the positrons present in the bulk because the lifetime of a positron before it annihilates with an electron is inversely proportional to the electron density at the site of annihilation. As shown later, the positrons trapped at vacancies and dislocations in the LPBF-fabricated 316L SS exhibit lifetimes of approximately 180 and 145 ps, respectively. The results of positron lifetime measurements indicate that vacancy-type defects are introduced during fabrication of the 316L SS and that the concentration of the introduced defects increases with scan speed of the LPBF process.

Next, a two-component analysis was performed using a trapping model with a fixed bulk positron lifetime of 104 ps. Fig. 2 shows that the relative intensity of the defect component increases with scan speed. The positron lifetime of the defect component averages out to 181.1 ps, which is consistent with the previously reported positron lifetime of vacancies in 316L SS (180 ps) [24]. Previous studies have also reported the presence of dislocation cells in LPBF-fabricated 316L stainless steel [8–19]. When different types of lattice defects are present in a material, identifying the recovery temperature of different lattice defects can lead to a more accurate analysis.

To understand the temperature-dependent recovery of lattice defects, the as-fabricated samples were isochronally annealed for 1 h, and positron lifetime measurements were performed after each annealing step. Fig. 3 shows that the positron lifetimes decrease with increasing annealing temperature. Notably, the positron lifetimes remain approximately 20 ps longer than that of the bulk positron lifetime (104 ps) at 573 K, which is the vacancy recovery temperature of 316L SS [24]. To identify the existing lattice defects after recovery of the vacancies at 573 K, a two-component analysis was performed on the positron lifetime spectra at 573 K. The average positron lifetime of the defect components at the recovery temperature was found to be 144.8 ps. The positron lifetime of the dislocations in the fabricated 316L SS was determined by performing positron lifetime measurements and component analyses on 1.1 % cold-rolled commercial samples of 316L SS; the average positron lifetime of the defect components was found to be 145.7 ps. Therefore,

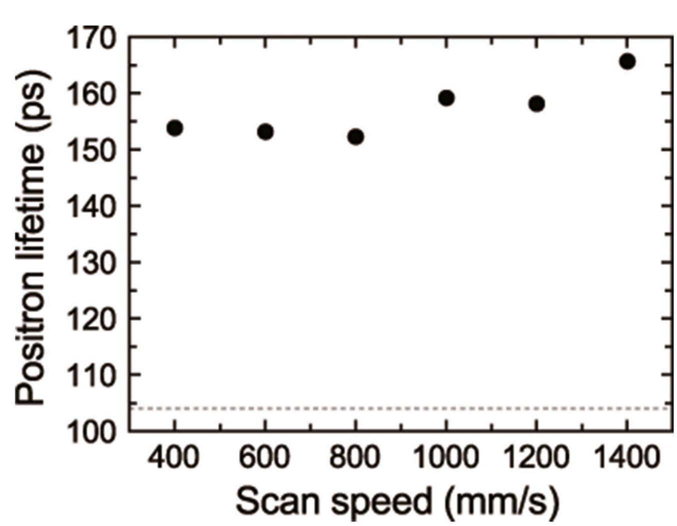

Fig. 1. Results of one-component analysis of the positron lifetime spectra of LPBF-fabricated 316L SS as a function of scan speed of the LPBF process. The dashed line represents the experimentally obtained bulk positron lifetime.

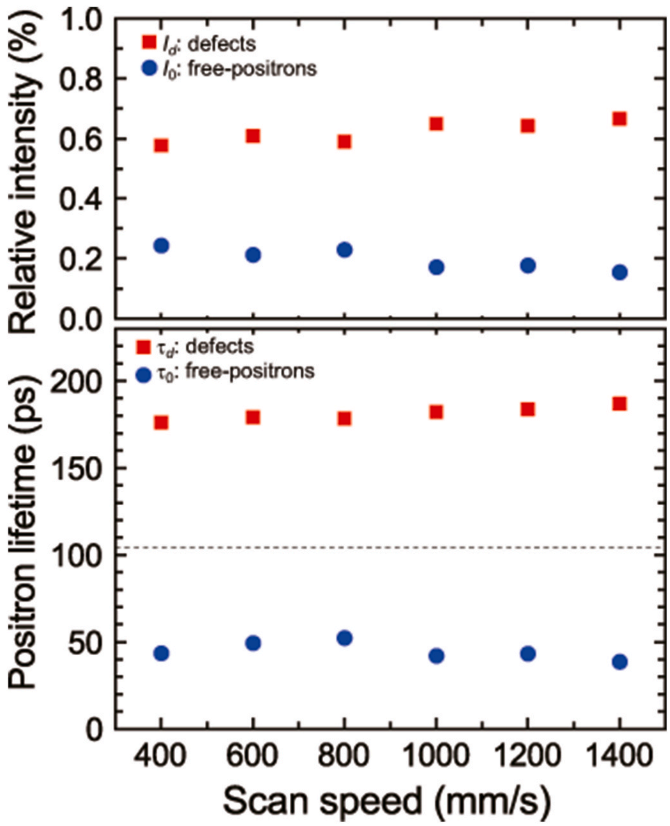

Fig. 2. Positron lifetimes and relative intensities derived using two-component analysis of the positron lifetime spectra of LPBF-fabricated 316L SS as a function of scan speed. The dashed line represents the experimentally obtained bulk positron lifetime.

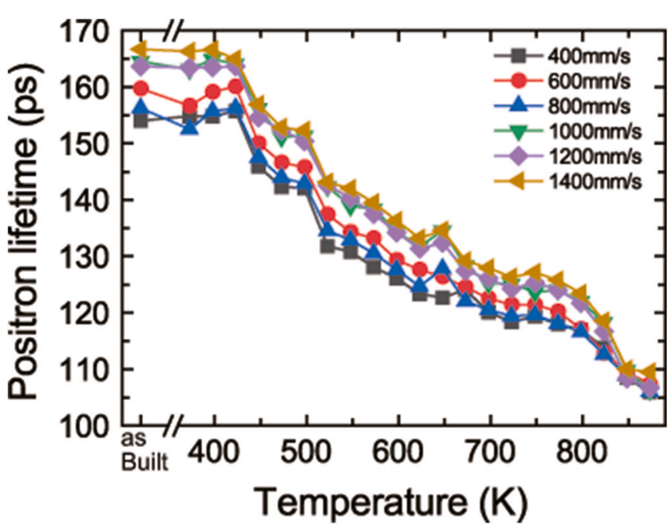

Fig. 3. Results of one-component analysis of the positron lifetime spectra of annealed 316L SS samples fabricated using different scan speeds of the LPBF process as a function of annealing temperature.

the observed positron lifetime of 144.8 ps after recovery of the vacancies in the 316L SS can be attributed to dislocations. Fig. 4 shows the results of three-component positron lifetime analysis on the 316L SS, fabricated at a scan speed of 400 mm/s, with the data plotted against annealing temperature. The results of three-component positron lifetime analysis were obtained by fixing the positron lifetimes of the vacancies and dislocations at 181.1 ps and 144.8 ps, respectively. The relative intensity

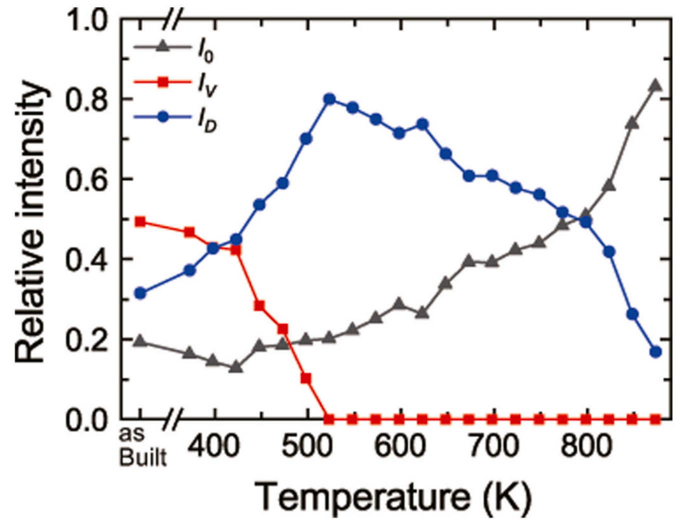

Fig. 4. Relative intensities derived using three-component analysis of the positron lifetime spectra of 316L SS fabricated at a scan speed of 400 mm/s as a function of annealing temperature.

of the vacancy component I_v sharply decreases above 423 K and eventually reduces to zero at 523 K (Fig. 4). The relative intensity of the dislocation component I_d increases up to 523 K, whereas that of the vacancy component decreases to zero at 523 K. The increase in the relative intensity of the dislocation component I_d up to 523 K does not indicate an increase in the dislocation density but is due to a decrease in the relative intensity of the vacancy component I_v as the vacancy concentration decreases.

The specific trapping rates of monovacancies and dislocations in pure iron are approximately 1.0×10^{15} s $^{-1}$ [25] and 5.1×10^{-5} m^2 s^{-1} [26], respectively. The vacancy concentrations and dislocation densities were calculated using the specific trapping rates of defects in iron. The results of one-component analysis in Fig. 1 show that the defect concentration in the LPBF-fabricated 316L SS increases with the scan speed of the LPBF process. The vacancy concentration in the as-fabricated 316L SS samples increases from 9.1 ppm to 23.9 ppm as the scan speed of the LPBF process increases from 400 mm/s to 1400 mm/s (Fig. 5(a)). Vacancy concentration in 316L SS at its melting point of 1673 K was estimated to be 14.1 ppm using an experimental vacancy formation energy of 1.61 eV [27]. The obtained results indicate that vacancies with concentrations comparable to those observed at the melting point are inherently present in LPBF-fabricated 316L SS. The vacancy concentration begins to steeply decrease at 423 K, reaching zero at 523 or 548 K. An increase in the dislocation density occurs up to 523 K or 548 K because the positrons trapped at vacancies began to be trapped at dislocations with decreasing vacancy concentration (Fig. 5(b)). Therefore, the dislocation density in the as-fabricated samples was obtained from the 316L SS samples immediately after the vacancies were recovered by annealing at 523 K or 548 K. In Fig. 6, both vacancy concentration and dislocation density can be observed to increase with increasing scan speed of the LPBF process. The increase in vacancy concentration can be attributed to the cooling rate, which increases as the scan speed of the LPBF process is increased [28,29].

The dislocation densities measured using the line-interception method on bright-field (BF) STEM images are presented in Fig. 7(a)–(c). The 316L SS samples fabricated at scan speeds of 400, 1000, and 1400 mm/s exhibit dislocation densities of 1.55×10^{14}, 1.84×10^{14}, and 3.36×10^{14} m^{-2}, respectively. These STEM results confirm that dislocation density increases with scan speed, consistent with previous measurements obtained under similar processing conditions (500–1300 mm/s, 240 W laser power) [16]. A prior study also reported that higher scan speeds promote greater dislocation content in LPBF-fabricated pure

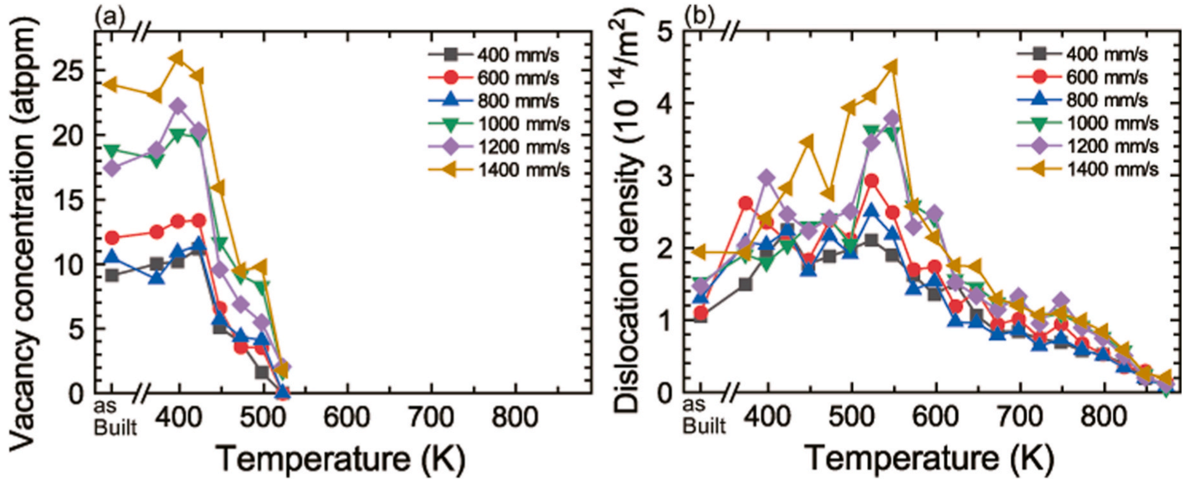

Fig. 5. (A) Vacancy concentration and (b) dislocation density in LPBF-fabricated 316L SS as a function of annealing temperature.

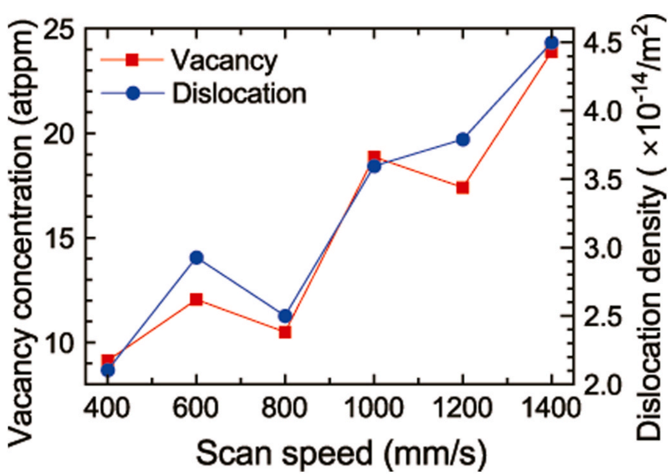

Fig. 6. Vacancy concentration and dislocation density in LPBF-fabricated 316L SS as a function of scan speed of the LPBF process.

molybdenum [30]. Earlier thermal stress analysis suggests that dislocations in additively manufactured materials primarily originate from deformation driven by thermal expansion and shrinkage under constrained conditions [10]. The present results further indicate that thermal distortions during LPBF increase with increasing scan speed, thereby contributing to the observed trend in dislocation density. Although the optimal levels of dislocations and vacancies in LPBF-fabricated 316L SS depend on the specific application and required properties, the findings of this study show that both features can be tailored through process parameters. Higher scan speeds lead to increases in both dislocation density and vacancy concentration. Conversely, if a reduced vacancy concentration is desired, post-build annealing at approximately 548 K can effectively decrease vacancy concentration while maintaining dislocation density.

Previous studies have extensively investigated the creep behavior of LPBF-fabricated 316L SS [31–36] because of its potential applications in high-temperature environments, such as those in power plants, nuclear reactors, and chemical processing industries. Different experimental results have been reported regarding the effect of dislocation cells on the creep behavior of LPBF-fabricated 316L SS. Li et al. reported that LPBF-fabricated 316L SS has a relatively shorter creep life than that of conventional 316 SS owing to the instability of the dislocation cell structure [32]. Pan et al. reported that LPBF-fabricated 316L SS exhibits

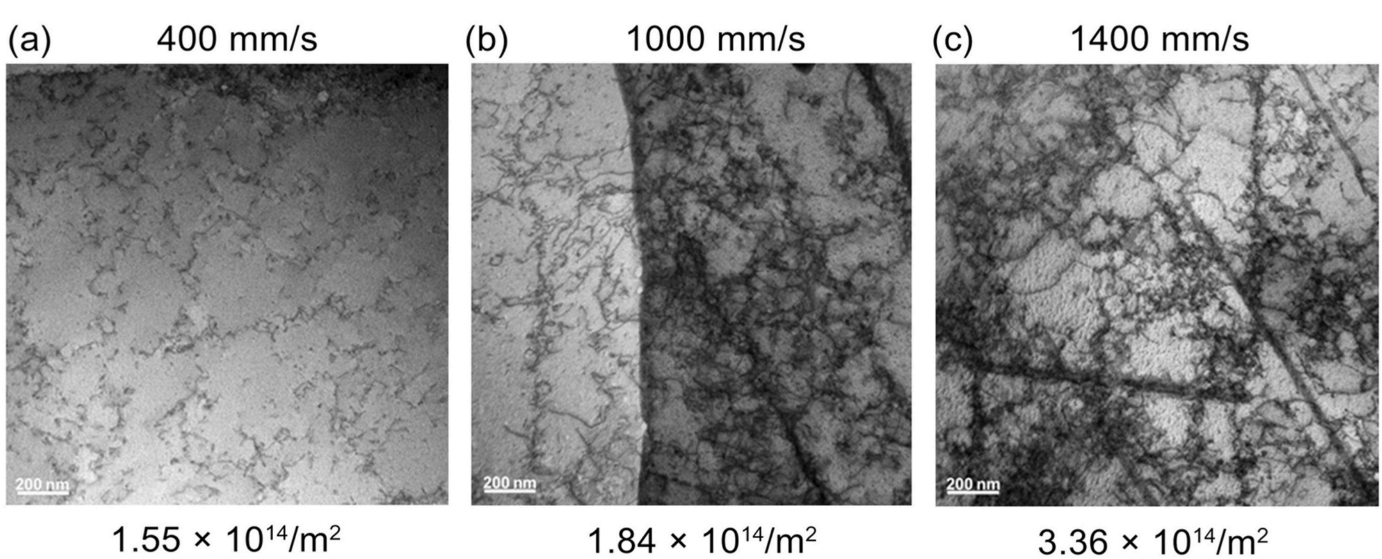

Fig. 7. BF-STEM images showing dislocation densities, obtained using the line-interception method, in 316L SS fabricated at a scan speed of (a) 400, (b) 1000, and (c) 1400 mm/s.

an extraordinary creep resistance, which is attributable to the hindered movement of the deformation-induced dislocations caused by stable dislocation cells [36]. The results of these studies suggest that the stability of dislocation cells in 316L SS depends on the parameters of the LPBF fabrication process.

Li et al. investigated the effect of heat treatment in the temperature range 923–1323 K on the creep behavior of LPBF-fabricated 316L SS and found that the creep life of 316L SS increases after heat treatment at 923 K and decreases with increasing heat treatment temperature [34]. Furthermore, Li et al. observed a decrease in the mean dislocation cell size and an increase in the dislocation cell wall thickness after heat treatment at 923 K and reported that these changes in the dislocation cell structure were associated with the increase in the creep life. Since quench-in vacancies are expected to be recovered by heat treatment at 923 K, the reduction of quench-in vacancies may contribute to the increased creep life of LPBF processed 316L SS. The results of molecular dynamics simulations on the creep in nanocrystalline 316L SS suggest that diffusion becomes the dominant mechanism during creep deformation of nanocrystalline 316L SS at relatively higher temperatures [37]. As previously discussed, vacancies at concentrations comparable to those at the melting point are inherently incorporated in LPBF-fabricated 316L SS. These quenched-in vacancies may contribute to accelerated creep deformation. On the other hand, for precipitation-hardening alloys, the quenched-in vacancies introduced in LPBF-fabricated samples may contribute to precipitation hardening by direct annealing without a prior solution treatment [38–42].

4. Conclusions

In this study, lattice defects in LPBF-fabricated 316L SS were characterized using positron lifetime measurements, revealing the presence of both monovacancies and dislocations in the as-fabricated condition. The vacancy concentration was found to be comparable to the thermal equilibrium vacancy concentration at the melting point. Increasing the scan speed during LPBF resulted in higher vacancy concentrations and dislocation densities, a trend further confirmed through TEM analysis. Post-processing experiments showed that quenched-in monovacancies were fully annealed out at 548 K, whereas dislocations persisted even after annealing above 800 K. These findings highlight the importance of understanding defect behavior over a range of temperatures to ensure that LPBF-fabricated 316L ss components achieve the required performance in high-temperature service environments.

CRediT authorship contribution statement

Masataka Mizuno: Conceptualization, Methodology, Investigation, Writing - original draft, Writing - review & editing. Masaki Otsuka: Investigation, Data curation, Visualization. Kazuhisa Sato: Investigation, Writing - review & editing. Takuya Ishimoto: Methodology, Validation, Investigation, Data curation, Writing - review & editing. Takayoshi Nakano: Conceptualization, Writing - review & editing, Supervision, Project administration, Funding acquisition. Hideki Araki: Conceptualization, Writing - review & editing, Supervision, Project administration, Funding acquisition.

Declaration of competing interest

The authors declare that they have no known competing financial interests or personal relationships that could have appeared to influence the work reported in this paper.

Acknowledgement

This work was supported by a Grant-in-Aid for Transformative Research Areas (A) on Creation of Materials by Super Thermal Field: Neo-3D printing by Manipulating Atomic Arrangement through Giant Potential Gradient (Grant number 21H05196) and a Grant-in-Aid for Scientific Research (C) (Grant number 23K04417) from the Japan Society for the Promotion on Science (JSPS). This work was also partially supported by CREST-Nanomechanics: Elucidation of macroscale mechanical properties based on understanding nanoscale dynamics for innovative mechanical materials (Grant Number: JPMJCR2194) from the Japan Science and Technology Agency.

Data availability

Data will be made available upon request.

References

[1] Jia Q, Rometsch P, Kürnsteiner P, Chao Q, Huang A, Weyland M, Bourgeois L, Wu X. Selective laser melting of a high strength: Al–Mn–Sc alloy: alloy design and strengthening mechanisms. Acta Mater 2019;171:108–18.
[2] Gu D, Shi Q, Lin K, Xi L. Microstructure and performance evolution and underlying thermal mechanisms of Ni-based parts fabricated by selective laser melting. Addit Manuf 2018;22:265–78.
[3] Puska MJ, Nieminen RM. Defect spectroscopy with positrons: a general calculational method. J Phys F Met Phys 1983;13:333–46.
[4] Sakaki K, Kawase T, Hirato M, Mizuno M, Araki H, Shirai Y, Nagumo M. The effect of hydrogen on vacancy generation in iron by plastic deformation. Scripta Mater 2006;55:1031–4.
[5] Sugita K, Mizuno M, Araki H, Shirai Y, Omura T, Tomatsui K, Sakiyama Y. Review of positron lifetime studies of lattice defects formed during tensile deformation in a hydrogen environment. ISIJ Int 2021;61:1056–63.
[6] Mizuno M, Sugita K, Do K, Ishimoto T, Nakano T, Araki H. Stability of vacancies in β-type Ti-15Mo-5Zr-3Al alloy fabricated via laser powder bed fusion. Addit Manuf Lett 2023;7:100162.
[7] Hu X, Lach TG, Terrani KA. Deuterium permeation and retention in 316L stainless steel manufactured by laser powder bed fusion. J Nucl Mater 2021;548:152871.
[8] Saeidi K, Gao X, Zhong Y, Shen ZJ. Hardened austenite steel with columnar sub-grain structure formed by laser melting. Mater Sci Eng A 2015;625:221–9.
[9] Wang YM, Voisin T, McKeown JT, Ye J, Calta NP, Li Z, Zeng Z, Zhang Y, Chen W, Roehling TT, Ott RT, Santala MK, Depond PJ, Matthews MJ, Hamza AV, Zhu T. Additively manufactured hierarchical stainless steels with high strength and ductility. Nat Mater 2018;17:63–71.
[10] Bertsch KM, de Bellefon GM, Kuehl B, Thoma DJ. Origin of dislocation structures in an additively manufactured austenitic stainless steel 316L. Acta Mater 2020;199: 19–33.
[11] Voisin T, Forien JB, Perron A, Aubry S, Bertin N, Samanta A, Baker A, Wang YM. New insights on cellular structures strengthening mechanisms and thermal stability of an austenitic stainless steel fabricated by laser powder-bed-fusion. Acta Mater 2021;203:116476.
[12] Cui L, Jiang S, Xu J, Peng RL, Mousavian RT, Moverare J. Revealing relationships between microstructure and hardening nature of additively manufactured 316L stainless steel. Mater Des 2021;198:109385.
[13] Yin H, Song M, Deng P, Li L, Prorok BC, Lou X. Thermal stability and microstructural evolution of additively manufactured 316L stainless steel by laser powder bed fusion at 500–800 °C. Addit Manuf 2021;41:101981.
[14] Sato K, Takagi S, Ichikawa S, Ishimoto T, Nakano T. Microstructure and solute segregation around the melt-pool boundary of orientation-controlled 316L austenitic stainless steel produced by laser powder bed fusion. Materials 2023;16: 218.
[15] Sun F, Ogawa T, Adachi Y, Sato K, Takagi S, Miyamoto G, Suzuki A, Yamanaka A, Nakada N, Ishimoto T, Nakano T, Koizumi Y. Modulated structure formation in dislocation cells in 316L stainless steel fabricated by laser powder bed fusion. Mater Trans 2023;64:1143–9.
[16] Liu W, Liu C, Wang Y, Zhang H, Li J, Lu Y, Xiong L, Ni H. Tailoring the microstructural and mechanical properties of 316L stainless steel manufactured by laser powder bed fusion. J Mater Res Technol 2023;25:7389–405.
[17] Fan J, Zhu Y, Wang W, Chen K, Godfrey A, Yu T, Huang X. Recovery of dislocation cell structures in 316L stainless steel manufactured by selective laser melting. J Mater Res Technol 2024;30:9472–80.
[18] Wang X, Nadimpalli VK, Tiedje NS, Jensen DJ, Yu T. Additive-manufacturing-induced cell structure in stainless steel 316L: 3D morphology and formation mechanism. Metall Mater Trans 2025;A56:506–17.
[19] Huang G, Chen H, Ma Z, Zhang R, Pei J, Lie Z, Du P, Peng X, Liu Y, Huang K. Microstructure and mechanical properties of stainless steel addictively manufactured via laser powder bed fusion in high-dense process parameter window. Mater Sci Eng 2025;A928:148033.
[20] Ishimoto T, Wu S, Ito Y, H Sun S-, Amano H, Nakano T. Crystallographic orientation control of 316L austenitic stainless steel via selective laser melting. ISIJ Int 2020;60:1758–64.
[21] Kirkegaard P, Eldrup M, Mogensen OE, Pedersen NJ. Program system for analysing positron lifetime spectra and angular correlation curves. Comput Phys Commun 1981;23:307–35.
[22] Kirkegaard P, Eldrup M. Positronfit extended: a new version of a program for analysing position lifetime spectra. Comput Phys Commun 1974;7:401–9.

[23] Seeger A. Investigation of point defects in equilibrium concentrations with particular reference to positron annihilation techniques. J Phys F Met Phys 1973;3: 248–94.
[24] Yabuuchi A, Maekawa M, Kawasuso A. Influence of oversized elements (Hf, Zr, Ti and Nb) on the thermal stability of vacancies in type 316L stainless steels. J Nucl Mater 2012;430:190–3.
[25] Vehanen A, Hautojärvi P, Johansson J, Yli-Kauppila J. Vacancies and carbon impurities in α- iron: electron irradiation. Phys Rev 1982;B25:762–80.
[26] Park YK, Waber JT, Meshii M, Snead Jr CL, Park CG. Dislocation studies on deformed single crystals of high-purity iron using positron annihilation: determination of dislocation densities. Phys Rev 1986;B34:823–36.
[27] Kim SM, Buyers WJL. Vacancy formation energies in bcc and fcc stainless steels by positron annihilation. Can J Phys 1983;61:140–5.
[28] Bertoli US, Guss G, Wu S, Matthews MJ, Schoenung JM. In-situ characterization of laser-powder interaction and cooling rates through high-speed imaging of powder bed fusion additive manufacturing. Mater Des 2017;135:385–96.
[29] Gokcekaya O, Ishimoto T, Hibino S, Yasutomi J, Narushima T, Nakano T. Unique crystallographic texture formation in Inconel 718 by laser powder bed fusion and its effect on mechanical anisotropy. Acta Mater 2021;212:116876.
[30] Ellsworth NE, Machacek JR, Kemnitz RA, Eckley CC, Sexton BM, Gearhart JA, Burggraf LW. Laser powder bed fusion of molybdenum and Mo-0.1SiC studied by positron annihilation lifetime spectroscopy and electron backscatter diffraction methods. Materials 2023;16:1636.
[31] Williams RJ, Al-Lami J, Hooper PA, Pham MS, Davies CM. Creep deformation and failure properties of 316 L stainless steel manufactured by laser powder bed fusion under multiaxial loading conditions. Addit Manuf 2021;37:101706.
[32] Li M, Zhang X, Chen WY, Byun TS. Creep behavior of 316 L stainless steel manufactured by laser powder bed fusion. J Nucl Mater 2021;548:152847.
[33] Ávila Calderón LA, Rehmer B, Schriever S, Ulbricht A, Agudo Jácome L, Sommer K, Mohr G, Skrotzki B, Evans A. Creep and creep damage behavior of stainless steel 316L manufactured by laser powder bed fusion. Mater Sci Eng 2022;830:142223.
[34] Li M, Chen WY, Zhang X. Effect of heat treatment on creep behavior of 316 L stainless steel manufactured by laser powder bed fusion. J Nucl Mater 2022;559: 153469.
[35] Ulbricht A, Ávila Calderón LA, Sommer K, Mohr G, Evans A, Skrotzki B, Bruno G. Evolution of creep damage of 316L produced by laser powder bed fusion. Adv Eng Mater 2023;25:2201581.
[36] Pan Y, Hu H, Wang K, Dong N, Qiu R, Wen JF, Song M, Tu ST. Creep behavior and fracture mechanism of an additively manufactured 316L stainless steel with extraordinary creep resistance. Mech Mater 2024;196:105053.
[37] Wang B, Wang Q, Luo R, Kan Q, Gu B. Atomistic study on high temperature creep of nanocrystalline 316L austenitic stainless steels. Acta Mech Sin 2023;39:122470.
[38] Marchese G, Lorusso M, Parizia S, Bassini E, Lee JW, Calignano F, Manfredi D, Terner M, Hong HU, Ugues D, Lombardi M, Biamino S. Influence of heat treatments on microstructure evolution and mechanical properties of Inconel 625 processed by laser powder bed fusion. Mater Sci Eng A 2018;729:64–75.
[39] Hadadzadeh A, Shahriari A, Amirkhiz BS, Li J, Mohammad M. Additive manufacturing of an Fe–Cr–Ni–Al maraging stainless steel: microstructure evolution, heat treatment, and strengthening mechanisms. Mater Sci Eng A 2020; 787:13947.
[40] Peng H, Wu S, Kan WH, Lim SCV, Zhu Y, Huang A. Rapid hardening response of ultra-hard Ti-6Al-2Sn-4Zr-6Mo alloy produced by laser powder bed fusion. Scripta Mater 2023;226:115209.
[41] Keya T, Bikmukhametov I, Shmatok A, Harvill G, Brewer LN, Thompson GB, Andurkar M, Thompson SM, O'Donnell V, Gahl J, Prorok BC. Evolution of microstructure and its influence on the mechanical behavior of LPBF inconel 625 upon direct aging. Manuf Lett 2023;35:732–42.
[42] Negron J, Ali M, Almotari A, Algamal A, Alafaghani A, Qattawi A. Impact of different heat treatments on the mechanical properties and microstructure of precipitation-hardened stainless steel fabricated by laser powder bed fusion. Metallogr Microstruct Anal 2024;13:317–31.